Title: Key Factors Improving Oxygen Reduction Reaction Activity in Cobalt Nanoparticles Modified Carbon Nanotubes

Authors: Atsushi Gabe, Jaime García-Aguilar, Ángel Berenguer-Murcia, Emilia Morallón, Diego Cazorla-Amorós

PII: S0926-3373(17)30534-9
DOI: http://dx.doi.org/doi:10.1016/j.apcatb.2017.05.096
Reference: APCATB 15740

To appear in: *Applied Catalysis B: Environmental*

Received date: 9-3-2017
Revised date: 26-5-2017
Accepted date: 31-5-2017

Please cite this article as: Atsushi Gabe, Jaime García-Aguilar, Ángel Berenguer-Murcia, Emilia Morallón, Diego Cazorla-Amorós, Key Factors Improving Oxygen Reduction Reaction Activity in Cobalt Nanoparticles Modified Carbon Nanotubes, Applied Catalysis B, Environmentalhttp://dx.doi.org/10.1016/j.apcatb.2017.05.096

Key Factors Improving Oxygen Reduction Reaction Activity in Cobalt Nanoparticles Modified Carbon Nanotubes

Atsushi Gabe[a], *Jaime García-Aguilar*[a], *Ángel Berenguer-Murcia*[a], *Emilia Morallón*[b], *Diego Cazorla-Amorós*[a,*]

[a] Departamento de Química Inorgánica and Instituto de Materiales. Universidad de Alicante, Ap. 99, 03080, Alicante, Spain

[b] Departamento de Química Física and Instituto de Materiales. Universidad de Alicante, Ap. 99, 03080, Alicante, Spain

---

<InlineShape8>

*Corresponding Author

E-mail address: cazorla@ua.es (D.C.A.).

Graphical Abstract

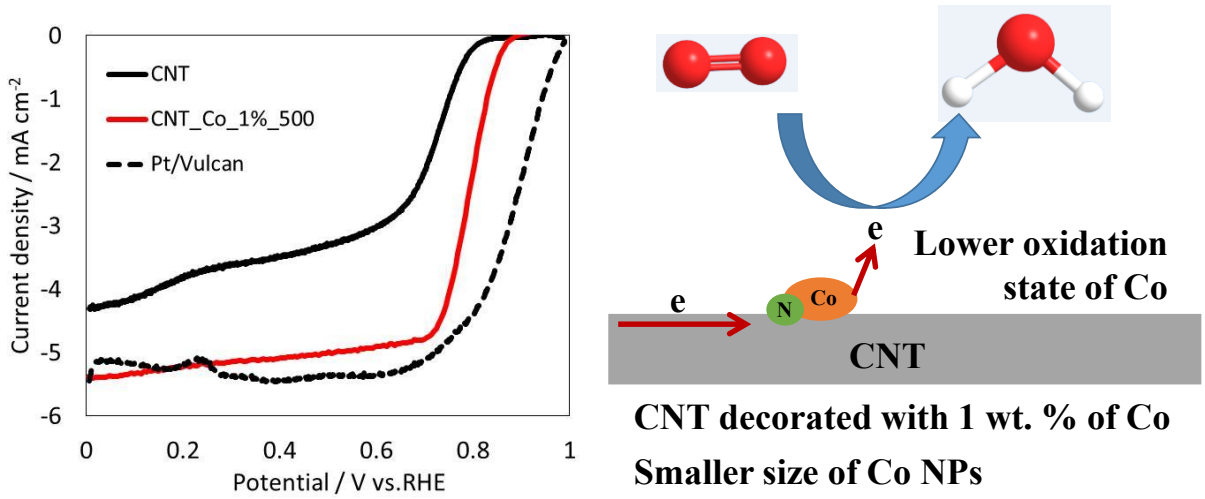

<InlineImage1>

Highlights

- CoO_x-N nanoparticles loaded on CNTs are prepared by a simple procedure
- CoO_x loading/nanoparticle size affects the electrocatalytic behaviour
- ORR activity is very much influenced by the N content in the electrocatalyst
- C-N-Co interactions are quite important for the remarkable electrocatalytic activity
- No significant deactivation is observed after MeOH addition with only 1 wt. % of Co

Abstract

Multiwall carbon nanotubes (CNTs) decorated with cobalt oxide (CoO_x) nanoparticles (NPs) are prepared in various synthesis conditions to investigate their capability as oxygen reduction reaction (ORR) catalysts for fuel cells in alkaline media. The synthesis conditions include the use of protecting, reducing or complexing agents and heat treatment. Higher ORR activity is possible for smaller size of Co NPs catalysts due to the enlarged interfaces between Co species and CNTs. The addition of polyvinylpyrrolidone (PVP) as protecting agent and $NaBH_4$ during the preparation procedure is necessary for obtaining the highest activity since it favors the formation of lower oxidation states for Co species and the incorporation of N groups which improve ORR activity. CNTs loaded with only 1 wt. % of Co NPs prepared by a facile method using PVP, $NaBH_4$ and subsequent heat treatment at 500ºC under N_2 atmosphere, demonstrates both similar catalytic

activity and stability than Pt/Vulcan (20 wt. % Pt on Vulcan). The synergic chemical coupling effects between CNTs and CoO_x NPs and the presence of carbon material with pyridinic N and quaternary N groups formed from the protecting agent decomposition, seem to be the main factors responsible for the remarkable electrocatalytic activity.

Keywords: Oxygen reduction reaction; electrocatalyst; CoOx nanoparticles; Carbon nanotubes; C-N-Co interaction

1. Introduction

Fuel cells (FCs) are electrochemical devices which transform directly the heat of combustion of a fuel (hydrogen, natural gas, methanol, ethanol, hydrocarbons, etc.) into electricity. The fuel is oxidized electrochemically at the anode, without producing any pollutants (only water and/or carbon dioxide are rejected in the atmosphere), whereas the oxidant (oxygen from the air) is reduced at the cathode. For instance, Alkaline Fuel Cells (AFCs) work with pure hydrogen and oxygen from room temperature to 80°C. Alkaline electrolytes such as KOH used in AFCs (usually in concentrations of 30–45 wt. %) have an advantage over acidic fuel cells, i.e., the oxygen reduction kinetics is much faster than in acidic media [1]. The power output and lifetime of FCs are directly linked to the behavior of the cathode, where most of the polarization losses occur, because the oxygen reduction reaction (ORR) is a slow reaction compared to the hydrogen oxidation at the anode. As a consequence, cathode development requires special attention to find the best catalyst and electrode structure to combine performance and stability [2,3]. Platinum (Pt) is the most commonly used and active electrocatalyst for the ORR and all of the Pt-group metals reduce oxygen in alkaline media according to the direct 4-electron process [3]. However, their large-scale commercial application has been precluded due to high cost of Pt. In addition, the Pt-

based electrodes suffer from low selectivity to ORR in the presence of other reactions (e.g., methanol oxidation derived from fuel crossover in FCs) and CO deactivation [2,4–6].

In contrast, the inherently faster kinetics of the ORR in alkaline media permits the use of non-noble metal catalysts as cathode electrodes [7,8]. In this sense, a wide range of catalysts including non-noble metals has been explored to replace the Pt-based cathode catalyst [3]. Indeed, metal-free heteroatom-doped carbon materials (N, S, P, B and F), transition metal oxides (e.g., CoO, Co_3O_4, Cu_2O, MnO_2) and metal nitrogen complexes (Co-N_x, Fe-N_x) on carbon nanomaterials can be promising candidates as non-precious metal catalysts [9–12].

Although transition metal oxides can be good materials for this application, unsupported metal oxide particles do not show a good performance at more negative potentials due to the poor transfer of substrate (O_2) and products (H_2O) [13], making necessary the synthesis of nanoparticles (NPs) supported on an adequate support like carbon materials. Carbon materials or nanomaterials are useful supports for non-noble metal-based systems, especially for those with low electrical conductivity. Furthermore, the carbon support can provide paths for the flow of electrons in the electrocatalytic system [14]. In this sense, new nanostructured carbon materials such as graphene and carbon nanotubes [15] have widely contributed to deriving advanced electrocatalysts due to their desirable electrical and mechanical properties as well as large surface area.

As non-noble metal catalyst, CoO_x (cobalt oxide)-based carbon catalysts are expected to be one of the promising alternatives to Pt-based electrocatalysts [16,17]. CoO_x supported on graphene and other carbon materials has been reported as highly active electrocatalysts for the ORR [13,18,19]. In order to improve the ORR catalytic activity and stability, some works have focused their research on CoO_x doped with N; for this reason various nitrogen containing ligands were used as precursors to form Co-complexes [20–22]. Liang et al. reported that NPs size of Co_3O_4 (~70 wt.

%) grown on nitrogen doped reduced graphene oxide (4–8 nm in size) were smaller than those grown on reduced graphene oxide without nitrogen doping (12–25 nm in size). While the pure Co_3O_4 or reduced graphene oxide alone have a very low catalytic activity, the hybrid material with smaller NPs exhibited an unexpectedly high ORR activity that was further enhanced by nitrogen doping of grapheme [21]. Another example was proposed by Yuan

et al. where a novel nanowire-structured polypyrrole-cobalt composite was successfully synthesized using cetyltrimetylammounnium bromide as surfactant [23]. This electrocatalyst showed a superior ORR performance than that of granular polypyrrole-cobalt catalyst prepared without the surfactant and also a better durability than the commercial 20 wt. % Pt/C catalyst. The high quantity of Co-pyridinic-N groups, which worked as ORR active sites, and its large specific surface area facilitated its ORR activity enhancement. Liu et al. investigated about the dependence of ORR activity on particle size of cobalt monoxides (CoO) and carbon composites [24]. Liu et al. prepared catalysts based on CoO (7 wt. %) supported on Vulcan, with an average size of 3.5, 4.9 and 6.5 nm, using a facile colloidal method avoiding any surfactants of long chain. It was concluded that the ORR activity is enhanced by the smaller CoO NPs due to enlarged interfaces between CoO and carbon materials [24].

Different oxidized phases of Co catalysts were prepared and their ORR activity were characterized by Liang et al. [25] Composites of CoO 40 wt. % on nitrogen doped carbon nanotube (NCNT) were obtained by thermal annealing of a mixture of $Co(OAc)_2$ and carbon nanotube at 400°C in NH_3/Ar atmosphere. Additionally, composites of Co_3O_4/NCNT and CoO_x/NCNT were also prepared by heat treatment in hydrothermal and Ar atmosphere, respectively. Among them, the CoO/NCNT hybrid showed higher ORR current density than Co_3O_4/NCNT and CoO_x/NCNT hybrids due to the strong interaction between the cobalt oxide and carbon material [25]. Uhlig et

al. prepared three plasma-treated (300, 450 or 600 W for 120 min) CoO_x catalysts supported on Vulcan containing ~20 wt. % of cobalt with a relatively homogeneous dispersion. Higher ORR activity was confirmed when using higher plasma treatment in KOH and K_2CO_3 electrolytes [26]. In summary, a variety of synthetic methods, conditions and carbon supports for Co modified carbon electrocatalysts have been explored for ORR. In this work, Multiwall carbon nanotubes (CNTs) loaded with different contents of Co NPs were prepared by a facile synthesis method consisting in a mixture of CNTs, a surfactant, a metal precursor (cobalt nitrate) and a reducing agent followed by their pyrolysis. Since the preparation method is able to determine the practicability and performance of electrocatalysts [10], several conditions were investigated to elucidate the relationships between properties of CoO_x, such as amount of CoO_x, NPs sizes, chemical composition and oxidation states of Co and ORR activities. Finally, a simple synthesis procedure of CoO_x NPs supported on CNTs that achieved high ORR catalytic activity with only 1 wt. % of Co NP is presented and insights into the factors governing the high catalytic activity are discussed.

2. Experimental Section

2.1 Preparation of CNTs

CNTs were purchased from Cheap Tubes Inc. (Brattleboro, Vt, USA) with a 95% of purity, outer diameter < 8 nm, length: 10-30 μm and a BET surface area of 484 m^2g^{-1}. Since some metal impurities can be present in the carbon material due to their synthetic procedure and they can affect the electrocatalyst activity [27,28], a purification treatment was performed to remove these impurities. The CNTs were purified by 1M hydrochloric acid solution for more than 12 hours (overnight) at room temperature followed by filtration and washing with distilled water. After the

acidic treatment, the CNTs were treated with 6M sodium hydroxide for 6 hours at 50°C to remove the residual ash content. The resulting CNTs were filtered and washed several times by distilled water until the pH of the filtrate was the same as that of the distilled water. Finally the material was dried at 120°C.

2.2 Decorating CoO_x nanoparticles on CNTs

For the preparation of the CoO_x-based CNTs materials, the following procedure was used. The necessary amount of Co precursor (cobalt(II) nitrate hexahydrate ($Co(NO_3)_2 \cdot 6\ H_2O$), Sigma-Aldrich) was dissolved in ethanol for a final nominal metal loading of 1, 9, and 17 wt. % of Co. Together with the Co precursor, the required amount of polyvinylpyrrolidone (PVP 40T, Sigma-Aldrich) were added to obtain a PVP/Co molar ratio of 10. After 2 hours under vigorous stirring, the purified CNTs were added to the solution. To favor the CNTs dispersion, the suspension was sonicated for 30s using an ultrasound probe (Bandelin Sonoplus GM2200, 200 W) at 25% output power. Afterwards, the suspension was stirred for 2 hours. The same sonication treatment was repeated before the addition of the reducing agent, sodium borohydride ($NaBH_4$, Sigma-Aldrich) at 0°C in an ice-bath. To ensure the total reduction of the Co(II), the suspension was stirred during 2 hours at 0°C followed by filtering and washing with ethanol. The prepared Co-based CNTs were dried at 80°C overnight. Finally, the obtained Co decorated CNTs were heat treated at 500°C under N_2 atmosphere for 1 hour to remove PVP [29]. In this study, the Co-based catalysts were named as CNT_Co_1%_500, in reference to the samples prepared with a nominal metal loading of 1 wt. % and treated under N_2 at 500°C during 1 hour. Some catalysts were tested without the N_2 heat treatment at 500°C.

For comparison purposes, additional Co-based CNTs were prepared modifying the described synthesis. One sample was prepared with a nominal metal loading of 1 wt. % without the presence

of PVP during the reduction step of the Co precursor. Furthermore, one sample was prepared without using the Co precursor but in the presence of PVP (CNT_PVP_500 sample). The nomenclature used for these samples are CNT_Co_1%_noPVP_500 and CNT_PVP_500, respectively. Moreover, another sample was prepared changing from the reduction agent ($NaBH_4$) to an ammonia solution (NH_4OH, 0.8 ml of 25 wt. %) to increase the pH and produce the precipitation of the Co oxide/hydroxides, as in a related work [24]. This sample is labeled as CNT_Co_1%_NH_3_500.

2.3 Characterization and electrochemical measurements

Transmission electron microscopy (TEM) images of the materials were taken with a JEOL JEM-2010 microscope operated at 200 kV. The samples were suspended in ethanol to obtain a homogeneous dispersion before drop-casting them on a copper grid and then placed in the measurement chamber. The amount of introduced CoO_x into the CNTs was examined by inductively coupled plasma-optical emission spectroscopy (ICP-OES). The ICP-OES results were obtained using a PerkinElmer Optima 4300 system. The samples were dissolved in 2 mL of concentrated aqua regia and filtered. The solutions were adjusted to a final Co concentration between 0-20 ppm for its determination in the linear signal range. The surface composition of the catalysts was investigated by using X-ray photoelectron spectroscopy (XPS) in a K-Alpha of Thermo-Scientific spectrometer, equipped with an Al anode. Elemental analysis of the surfaces was calculated from the areas under the main peak of each atom. Deconvolution of the XPS were done by least squares fitting using Gaussian-Lorentzian curves, and as the background determination, a Shirley line was used. X-ray diffraction (XRD) measurements were performed using Cu Kα radiation on a Bruker D8 Advance diffractometer.

Electrochemical activity tests towards ORR were carried out in a three-electrode cell using 0.1M KOH electrolyte, a Pt wire as counter electrode and Reversible Hydrogen Electrode (RHE) electrode as reference electrode. A rotating ring-disk electrode (RRDE, Pine Research Instruments, USA) equipped with a glassy carbon (GC) disk (5.61mm diameter) and a attached Pt ring was used as working electrode. The catalysts were dispersed in a solution of 75 vol. % of isopropanol, 25 vol. % of water and 0.02 vol. % of Nafion@ to prepare a final dispersion of 1 mg/ml of the CoO_x-CNTs material. Typically, 100 µl (mass of electrode is 400 µg/cm^2) of the dispersion was pipetted on a GC electrode to obtain uniform catalysts layer for ORR study although the effect of the mass of electrode (80, 800 and 1600 µg/cm^2) was also studied. The sample on the GC was dried by heating lamp for evaporation of the solvent. Cyclic Voltammetry (CV) and linear sweep voltammetry (LSV) were carried out from 0 to 1 V (vs. RHE). The CV was performed in both N_2 and O_2 saturated atmosphere at 50 mVs^{-1}. The LSV was done in an O_2-saturated atmosphere for different rotation rates of 400, 625, 900, 1025, 1600 and 2025 rpm at 5 mVs^{-1}. The potential of the ring was kept at 1.5 V (vs. RHE) and the ring current by H_2O_2 oxidation was also measured during the LSV measurement. The electron transfer number (n) of ORR on the catalysts modified electrode was determined by the following equation [30].

$$n = \frac{4 \times Id}{Id + Ir/N} \quad (1)$$

where Id is disk current, Ir is ring current, and N is the collection efficiency of the ring which was experimentally determined to be 0.37.

3. Results and Discussion

3.1 Chemical characterization

Table 1 shows the Co content in the prepared catalysts determined by ICP-OES analysis. These results reveal that CoO_x loading on CNTs was successful and samples with sufficiently different Co contents were prepared. However, the amount of Co obtained for the highest Co contents were lower than the intended values probably due to the lack of adequate interaction between the CNTs surfaces and the Co NPs reactants or the limited surface area of CNTs. In this study, we will maintain in the nomenclature the nominal content of Co although the results, if necessary, will be referred to the real Co content of the catalysts.

Table 2 shows nitrogen atomic composition obtained from XPS (XPS survey spectra and C, N and O atomic compositions for prepared catalysts are shown in Fig. S1 and Table S1, respectively). The catalysts prepared with PVP presents a detectable nitrogen content while for CNT and CNT_Co_1%_noPVP_500 nitrogen was not detected. This is because PVP decomposition during catalyst pretreatment may produce some carbon material which introduces some N doping near Co atoms since PVP molecules are initially coordinating Co atoms on the NPs surface. Specifically, the catalysts prepared with $NaBH_4$ reveal a relatively higher amount of nitrogen than that prepared with NH_3 (Table 2).

Fig. 1 represents the high-resolution Co 2p and N 1s XPS spectra for a selection of CoO_x decorated catalysts. The two peaks at binding energies (BE) around 780 eV and 795 eV are related to Co 2p(3/2) and Co 2p(1/2), respectively [31]. Although the Co(II) and Co(III) sites have similar 2p BE, they can be differentiated when Co_3O_4 species are formed. The BE of Co(II) is found to be at 781.3 eV for Co 2p(3/2) and 797.3 eV for Co 2p(1/2), whereas the BE of Co(III) is at around 780.0 eV for Co 2p(3/2) and 795.1 eV for Co 2p(1/2) [13,31]. The deconvolution profiles in Fig. 1 show that the oxidation state of Co on the catalysts prepared herein was mainly Co(II). Fig. 1a contains well defined Co(II) peaks for Co 2p(3/2) as well as Co 2p(1/2) for catalysts CNT_Co_1%_500,

CNT_Co_9%_500 and CNT_Co_17%_500. In addition, strong satellite peaks at around 785.5 and 804.2 eV presenting 6 eV above the primary spin-orbit BE were observed. These peaks reveal another proof for high-spin Co(II) species [10,32]. Moreover, Co metallic peak at around BE of 778 eV and 793.3 eV were detected for CNT_Co_1%_500, CNT_Co_9%_500 and CNT_Co_17%_500 catalysts [33,34]. In contrast, as shown in Fig. 1b, no clear Co 2p peaks, especially for Co 2p(1/2), are observed for 1 wt. % of Co-containing catalyst synthesized without PVP followed by heat-treatment (CNT_Co_1%_noPVP_500). Interestingly, metallic Co was not detected for CNT_Co_1%_NH_3_500 but the XPS suggests the presence of Co(III) species. In summary, XPS shows that in the synthesis method in which PVP and the reducing agent are used, most of the Co remains as Co(II) together with small amounts of metallic Co. If the reducing agent is not used, Co(III) species are detected. Fig. S2 shows the XRD patterns of CNT, CNT_Co_1%_500, CNT_Co_9%_500, CNT_Co_17%_500 and CNT_Co_1%_NH_3_500. CNT_Co_9%_500 and CNT_Co_17%_500. Peaks associated to CoO and Co are only barely observable for the samples with the highest Co content, indicating the existence of both CoO and Co species in these catalysts. However, for the samples with the lowest Co content (CNT_Co_1%_500 and CNT_Co_1%_NH_3_500) no clear features are distinguished due to the low amount of Co and the small particle size.

Fig. 1c includes the high resolution XPS spectra for N 1s of CNT, CNT_Co_1%_noPVP_500, CNT_Co_1%_500, CNT_Co_9%_500, CNT_Co_17%_500 and CNT_Co_1%_NH_3_500. The spectra of CNT_Co_1%_500, CNT_Co_9%_500, CNT_Co_17%_500 and CNT_Co_1%_NH_3_500 could be deconvoluted into three peaks with maxima at 398.5, 399.8 and 401.5 eV which indicate pyridinic N, pyrrolic/pyridonic N and quaternary N, respectively [12,23,35,36]. The content of different N species for the catalysts are also indicated in Table 2.

Larger N content and more pyridinic N and quaternary N species were detected in samples CNT_Co_1%_500, CNT_Co_9%_500 and CNT_Co_17%_500 than CNT_Co_1%_NH_3_500. To sum up, the preparation protocol using $NaBH_4$ favors the formation of pyridinic N and quaternary N groups as well as a higher amount of nitrogen content.

<InlineShape1>

(c)

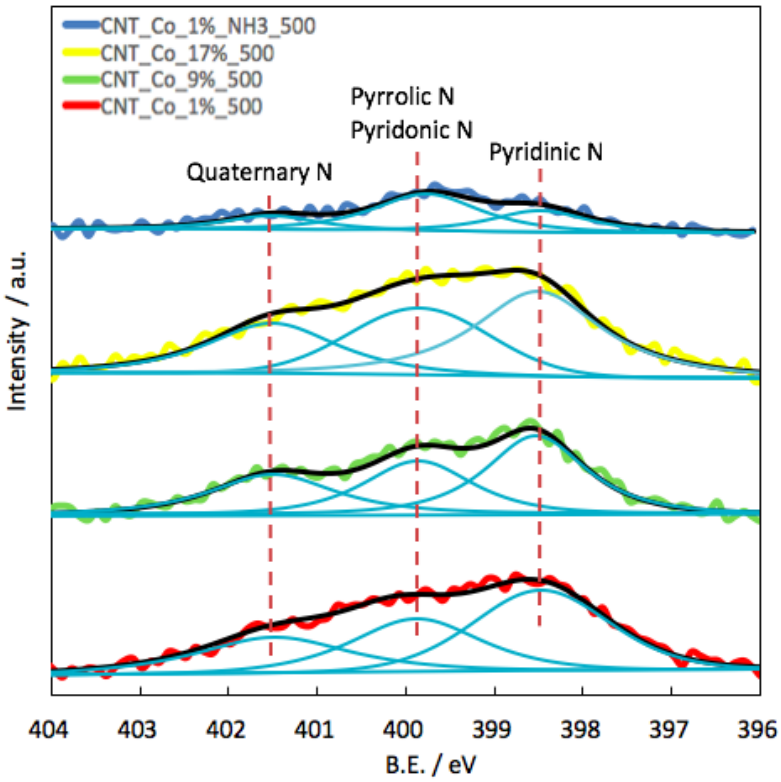

Fig. 1. Co 2p spectra of (a) CNT, CNT_Co_1%_500, CNT_Co_9%_500 and CNT_Co_17%_500 (b) CNT_Co_1%_500, CNT_Co_1%_NH_3_500 and CNT_Co_1%_noPVP_500. (c) N 1s spectra of CNT_Co_1%_500, CNT_Co_9%_500, CNT_Co_17%_500 and CNT_Co_1%_NH_3_500.

Fig. 2 shows the TEM images for catalysts with different amounts of Co but prepared with the same method (CNT_Co_1%_500, CNT_Co_9%_500 and CNT_Co_17%_500) and 1 wt. % of Co-containing catalysts prepared by different synthesis methods (CNT_Co_1%_noPVP_500 and CNT_Co_1%_NH_3_500). About 100 particles are randomly selected for the analysis of CoO_x NPs size distributions. Average NPs size increases with increasing Co content following the same preparation method. However, it remains nearly constant when 1 wt. % of Co is loaded using different preparation methods. These TEM results indicate that the concentration of Co in the catalysts has a greater contribution in the particle size of Co NPs than the chemical agents used in the synthesis. In addition, Fig. 2f represents high resolution TEM image of CNT_Co_17%_500 as an example of the prepared catalysts using PVP and $NaBH_4$. As shown in Fig. 2f, a thin deposit is observed around the CoOx NPs which could be due to the PVP carbonization which may contain most of the N species detected.

<InlineShape3>

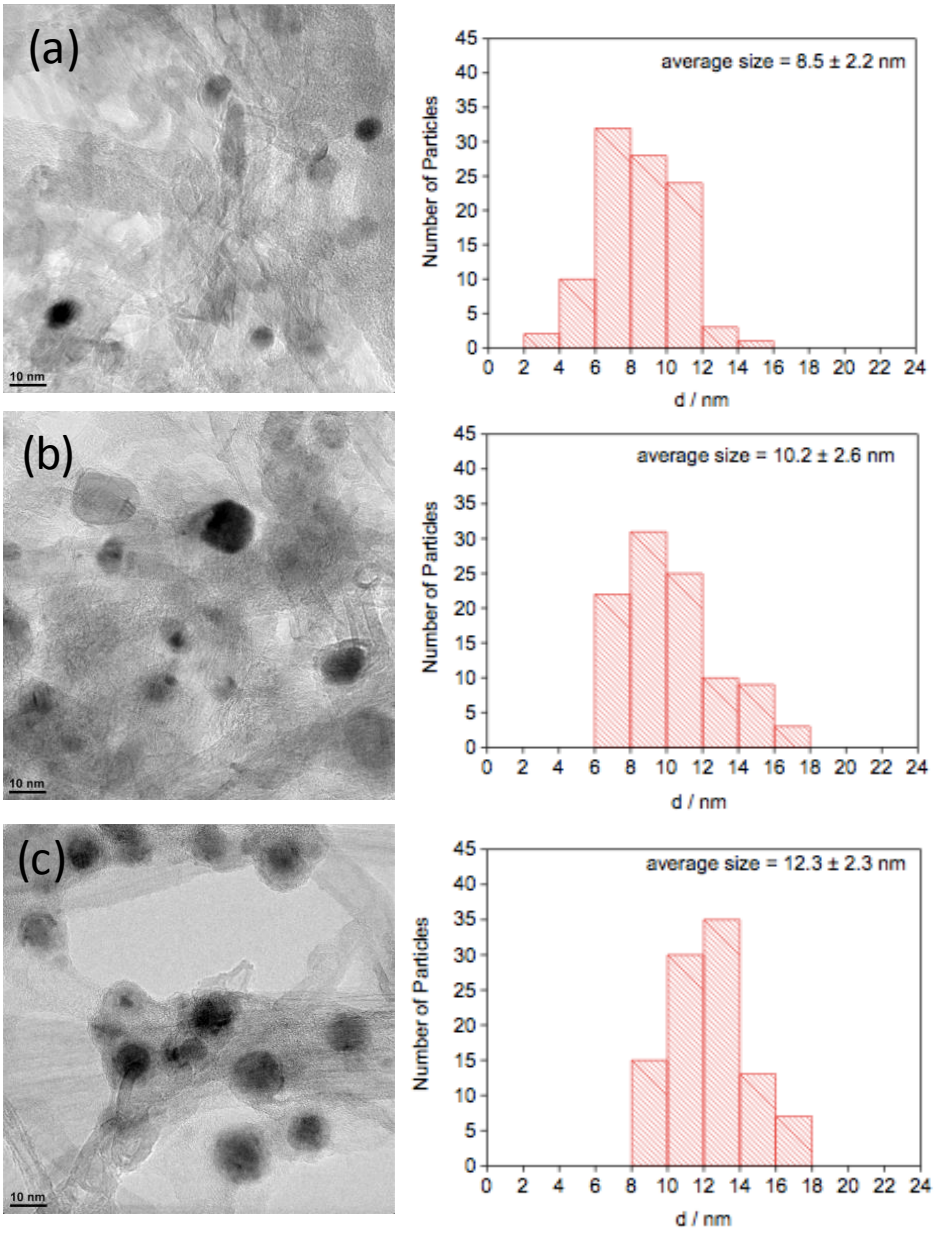

<InlineSha

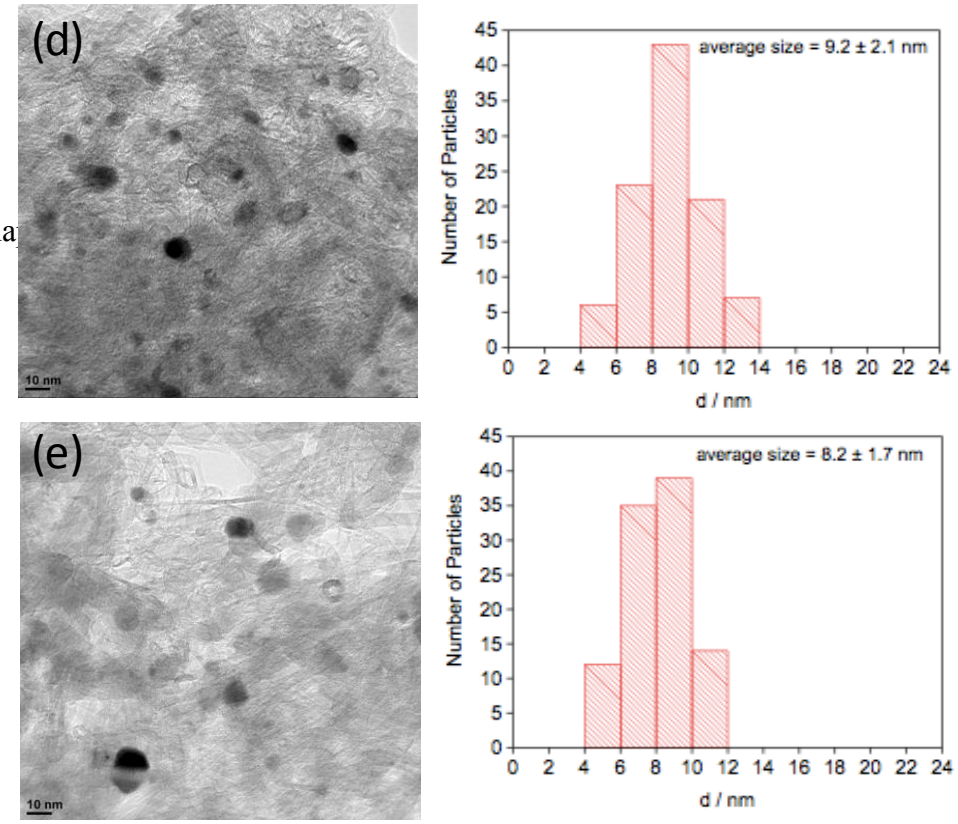

<InlineShape5>

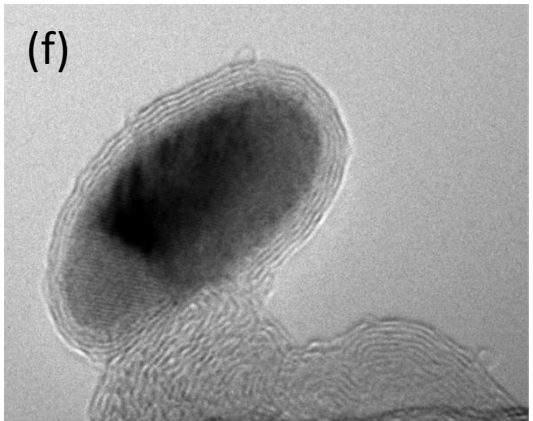

Fig. 2. TEM images of (a) CNT_Co_1%_500, (b) CNT_Co_9%_500, (c) CNT_Co_17%_500, (d) CNT_Co_1%_noPVP_500 and (e) CNT_Co_1%_NH_3_500. TEM image of (f) CNT_Co_17%_500 with high resolution.

3.2 Electrochemical characterization

The ORR catalytic activity of the Co-containing samples was preliminary characterized by CV under N_2 and O_2 saturated atmosphere in 0.1M KOH. The CV curves for CNT, CNT_Co_1%_500 and CNT_Co_17%_500 in N_2 and O_2 saturated atmosphere are shown in Fig. 3a, 3b and 3c respectively. The oxidation current observed for CNT_Co_17%_500 at potentials higher than 0.8 V vs RHE (Fig. 3c), can be associated to the oxidation of Co(II) to Co(III) according to the following reaction: $3Co^{2+} + 8OH^- \rightarrow Co_3O_4 + 4H_2O + 2e^-$ [25,37]. This oxidation current is not clearly observed for sample CNT_Co_1%_500 due to the low Co content. The CV curves in Fig. 3b in presence of O_2 show the reduction peak for O_2, which has a more positive onset potential for CNT_Co_1%_500 and CNT_Co_17%_500 than CNT. Moreover, the CNT_Co_1%_500 sample exhibits much higher reduction current than CNT_Co_17%_500.

To quantitatively investigate the ORR performance, experiments with a RRDE were performed. Fig. 4 represents LSVs and current during ORR for disk and ring electrodes at different rotating rates on CNT and CNT_Co_1%_500 catalysts. The Limiting Current (LC) increased with increasing the rotating rate due to shortened diffusion distance at high rotating rate [20]. CNT_Co_1%_500 showed wide current plateau and much higher LC as well as onset potential compared to CNT. These results imply that the addition of CoO_x can significantly enhance the ORR activity. Similarly, the measured ring current which corresponds to the oxidation of hydrogen peroxide produced during the LSV curves in the disk electrode (divided by collection efficiency, 0.37) also increased with rotation rate as shown in Fig. 4. CNT_Co_1%_500 demonstrated lower ring current than CNT which indicates the formation of lower amount of hydrogen peroxide.

Fig. 5 presents the LSVs during ORR and electron transfer number (n) of the CNT, CNT_Co_1% (without heat treatment under N_2 at 500˚C), CNT_Co_1%_500 and Pt/Vulcan (20 wt. % Pt on Vulcan) catalysts measured at an electrode rotating rate of 1600 rpm with a potential scanning rate of 5 mV/s. The heat-treatment at 500°C under N_2 was performed to remove the PVP from the catalysts [29]. As shown in Fig. 5, the catalyst without heat-treatment (CNT_Co_1%) has much lower LC and n than CNT. This is because the remaining PVP in the catalyst hinders the accessibility of oxygen to the active sites for ORR. However, the onset potential as well as LC of the CNT_Co_1%_500 were dramatically improved, while the selectivity of the reaction towards water formation was also enhanced. The CNT_Co_1%_500 reached LC of -5.7 mA/cm^2 which is similar to that observed for Pt/Vulcan catalyst.

In order to clarify the influence of the PVP toward ORR activity, catalysts were also prepared without PVP (with Co precursor) or without Co precursor (with PVP). Fig. 6 presents the ORR

currents for the CNT, CNT_PVP_500, CNT_Co_1%_500 and CNT_Co_1%_noPVP_500 measured at an electrode rotating rate of 1600 rpm with a potential scanning rate of 5 mV/s. The LC and n of the catalyst without PVP were higher than that of CNT. However, LC and n of CNT_Co_1%_noPVP_500 were not as much enhanced as CNT_Co_1%_500. Especially, LC of catalyst prepared without PVP showed a significantly lower value than that of CNT_Co_1%_500. Likewise, LC and n of the catalyst prepared without Co precursor (CNT_PVP_500) were not highly improved as CNT_Co_1%_500 showed, which implies that the effect of PVP toward ORR is negligible when the Co is not present on CNT.

These results reveal that PVP plays an important role during the synthesis of Co-containing catalyst, either favoring the formation of well dispersed NPs or introducing some electronic or chemical changes on the catalytic species. It is well known that PVP acts as a protecting agent of the colloidal particles preventing agglomeration. This has been manifested in different NPs composition like Pd nanoparticles and Sn-3.5Ag alloy NPs [29,38]. However, TEM images in Fig. 2 do not show relevant differences between both catalysts in terms of average particle size, suggesting that this is not the main factor explaining the effect of PVP.

On the other hand, as demonstrated in XPS N1s in Figure 1c and TEM image in Figure 2e, PVP decomposition during catalyst pretreatment produces a N-doped carbon shell on Co NP. Moreover, Fig.1c shows that pyridinic-N and quaternary N groups are present on CNT_Co_1%_500. The presence of these Co-N-C species constitute active sites which facilitate the adsorption of oxygen, leading to improved ORR performance as it has been proposed by other authors [12,23]. It must be emphasized that when PVP is not used this carbon shell is not formed and N is not detected, which results in a lower activity of the Co-containing catalyst.

Different amounts of CoOx NPs loaded on CNTs have been prepared to identify their effect on ORR activity. The ORR current densities and n of the catalysts with different Co contents (1, 9 and 17 wt. %) have been studied (Fig. S3 in Supplementary Data). The relationship between the Co content in the catalyst and LC as well as n at 0.3 V and 0.7 V (vs RHE) are summarized in Fig. 7. Remarkably, LC and n of the catalyst with 1 wt. % of CoO_x showed the highest values. As shown in Fig. 7a, the LC increased significantly up to a Co content of 1 wt. %, above which it decreased. The correlations of n and Co content in Fig. 7b presented similar behavior as LC. As displayed in Fig. 2, the average CoO_x NPs size follows the order of CNT_Co_17%_500 (13.1 nm) > CNT_Co_9%_500 (10.8 nm) > CNT_Co_1%_500 (8.9 nm). In contrast, LC and n follow the order CNT_Co_1%_500 > CNT_Co_9%_500 > CNT_Co_17%_500. In this sense, the results suggest that as the size of CoO_x NPs decreased, their ORR activities increased, which can be explained considering that ORR activity is enhanced by the smaller CoO_x NPs due to the enlarged interface between CoO_x and CNTs [24].

Though the LC of CNT_Co_1%_500 at 0.3 V (vs RHE) were similar to Pt/Vulcan (similar activity), the n value (~3.5) was lower than that of Pt/Vulcan (~4.0). It means that selectivity of CNT_Co_1%_500 is lower than Pt/Vulcan and follows a mix of a two and four electron pathway [26]. An associative pathway has been recently elucidated over CoO_x/C catalyst, which involves the following reactions: (i) $O_2 + H_2O + 2e^- \rightarrow HO_2^- + OH^-$; (ii) $HO_2^- + H_2O + 2e^- \rightarrow 3OH^-$ and (iii) $2HO_2^- \rightarrow O_2 + 2OH^-$. The interface between carbon and Co NPs can be identified as the most active sites for the first $2e^-$ reduction of oxygen to form HO_2^- [39]. Amount of active sites, which are responsible for reaction (i) in Co-containing catalysts, are larger than the amount of active sites for $4e^-$ electron pathway on Pt/Vulcan and thus, high LC for CNT_Co_1%_500 are obtained. In fact, the LC values are similar to Pt/Vulcan catalyst with a 20 wt. % of Pt in spite of the fact that

the Co catalyst has only 1 wt. %. Thus, it might be explained that the first two electrons pathway reaction (i) $O_2 + H_2O + 2e^- \rightarrow HO_2^- + OH^-$ proceeds efficiently for CNT_Co_1%_500 due to their smaller Co NPs size which results in a larger interface between Co species and carbon producing a much higher amount of HO_2^- [24].

In addition, Bonakdarpour et al. [40] reported that when the catalyst loading is low enough, the H_2O_2 molecules have a higher probability of diffusing away into the electrolyte than being reduced to water at a nearby site through reaction (ii). Therefore, the percentage of H_2O_2 released into the electrolyte strongly depends on the amount of electrocatalyst used on the RRDE [40]. Fig. 8 shows the ORR current densities and ring current densities as well as n for the CNT_Co_1%_500 measured for different loadings at rotation speed of 1600 rpm. At all potentials, the LC and n increased when larger loadings are used. At 1600 μg/cm^2, well defined mass transfer LC plateau of -6 mA/cm^2 as well as higher n (selectivity) was observed, probably indicating that close to four electrons are being generated for each oxygen molecule reaching the electrode through reaction (i) on the interface and (ii) $HO_2^- + H_2O + 2e^- \rightarrow 3OH^-$ on the Co NPs surface [24]. As revealed in Fig. 8, the HO_2^- yield decreased with increasing the loading (thickness) of the catalyst over the GC electrode.

Additional experiments were designed to investigate about the effect of $NaBH_4$ towards ORR activity. Instead of $NaBH_4$, 1 wt. % of Co decorated catalysts synthesized with NH_3 were prepared. Two advantages for using NH_3 can be mentioned: first, the ammonia molecules tend to be strongly bonded to cobalt cations, working as a capping agent to hinder particle growth; second, the hydrolysis rate of cobalt salt can be well controlled by ammonia which releases hydroxyl ions [21,24]. Fig. 9 shows LSV curves for ORR and n for the catalysts prepared with and without NH_3.

The LC of CNT_Co_1%_NH_3_500 is much lower than that of CNT_Co_1%_500. Fig. 2a and 2e show that the average CoOx NPs sizes of CNT_Co_1%_500 and CNT_Co_1%_NH_3_500 are about 9 nm. This means that Co NPs size of the catalysts prepared with NH_3 or $NaBH_4$ are very similar. It can be mentioned that not only Co NPs sizes but also the catalyst preparation procedure affects the ORR activity. According to the results of catalysts prepared herein, contribution towards ORR activity of catalysts prepared using $NaBH_4$ was higher than that of NH_3.

The XPS results show three important differences among the two samples: (i) Fig. 1b suggests the presence of Co(II) and Co(III) for CNT_Co_1%_NH_3_500, probably forming Co_3O_4 species, when $NaBH_4$ is not used; (ii) metallic Co is observed when $NaBH_4$ is used and (iii) pyridinic-N and quaternary N groups improving ORR performance are present in all the catalysts prepared with $NaBH_4$ (see Fig. 1c and Table 2). Thus, it seems that the interaction of reduced Co with PVP is more efficient making that some Co-N species which work as active sites for ORR are formed after the heat treatment.

Dong et al. reported that Co^{2+} ions coordinated with NH_3 form $[Co(NH_3)_6]^{2+}$ ions and most them were immediately oxidized to $[Co(NH_3)_6]^{3+}$ by O_2 according to the reaction $4[Co(NH_3)_6]^{2+} + O_2 + 2H_2O = 4[Co(NH_3)_6]^{3+} + 4OH^-$; then, after heat treatment Co_3O_4 nanomaterials are obtained [41]. Therefore Co(III) could be detected on CNT_Co_1%_NH_3_500. Liang et al. suggested that the carbon hybrid materials prepared with CoO contain larger amount of effective active or accessible ORR active sites than the carbon hybrid materials containing Co_3O_4 [25]. Furthermore, Xiao et al. investigated the relationship between surface structure of various types of cobalt oxide nanoparticles and their ORR activities [42]. It was concluded that the catalytically active sites for ORR should be the surface tetrahedral Co(II) sites.

Regarding metallic Co, it must be mentioned that Co(II) or Co(III) cannot be reduced in absence of $NaBH_4$. Actually, Co metallic was not found in other catalysts prepared with NH_3 which is in agreement with our results [21,22]. Wang et al. showed that in the catalysts with N-doped reduced graphene oxide aerogel (NGA), CoO and Co (CoO/Co-NGA) subunits had higher ORR activity than the catalysts without Co metallic (CoO-NGA) composites [43]. Highly integrated NGA, CoO and Co, suggests strong bonding between them, which would enhance the interaction between the metal oxide NPs and the graphene support, promoting electron and charge transfer among the active sites. Finally, the presence of Co-pyridinic-N and quaternary N groups, formed through the interaction of PVP and Co during the NPs synthesis when $NaBH_4$ is used, result in higher catalytic activity species as indicated by other authors [12,23].

In summary, different factors contribute to the optimum catalytic activity of Co NPs supported on nanostructured carbons. On the one hand, particle size has an important role since lower particle size results in larger amount of Co-Carbon interface sites. On the other hand, the Co-species composition has an important contribution since the presence of lower oxidation state Co sites and Co-N species results in enhanced catalytic activity when comparing catalysts with similar particle size.

3.3 Durability tests

The durability of an ORR catalyst is a factor which determines the life of a fuel cell [9]. The stability of the Co-containing catalyst was measured by RDE chronoamperometry under steady state mass transport conditions (0.65 V vs RHE). Fig. 10 shows the stability of the CNT_Co_1%_500 and Pt/Vulcan catalysts on normalized current base. The current density calculated on Co and Pt content in molar basis is also included in Fig. 10. Additionally, methanol poisoning test was performed by adding 1M methanol into the electrolyte after 2 hours reaction

[31]. As shown in Fig. 10, even after adding methanol, CNT_Co_1%_500 catalyst activity is more than 80% of the initial value over 3 hours. However, the current of the Pt/vulcan dropped to zero immediately after addition of methanol. The experiment supports that the Co-containing catalysts are suitable in terms of stability and resistance towards methanol. Furthermore, the current of CNT_Co_1%_500 per mole of metal content is higher than for Pt/Vulcan, showing that it is possible to achieve higher current densities than for Pt based catalysts with very low amounts of CoO_x (i.e., 1 wt. % in this study). In addition, potential cycling durability tests were carried out by cyclic voltammetry. The cycling was repeated under O_2-saturated 0.1M KOH solution at 50 mVs^{-1} from 0 to 1 V (vs.RHE) for 500 cycles. Fig.11 presents the LSV curves before and after the 500 cycling (LSV curve after 100 cycles is indicated only for CNT_Co_1%_500). As demonstrated in Fig.11, the half-wave potential for CNT_Co_1%_500 and Pt/Vulcan catalysts shifted to lower potentials by only 5 mV and 15 mV after 500 cycles, respectively. These results imply that our catalysts show good stability in alkaline solution which means that they are interesting as catalysts for alkaline fuel cells.

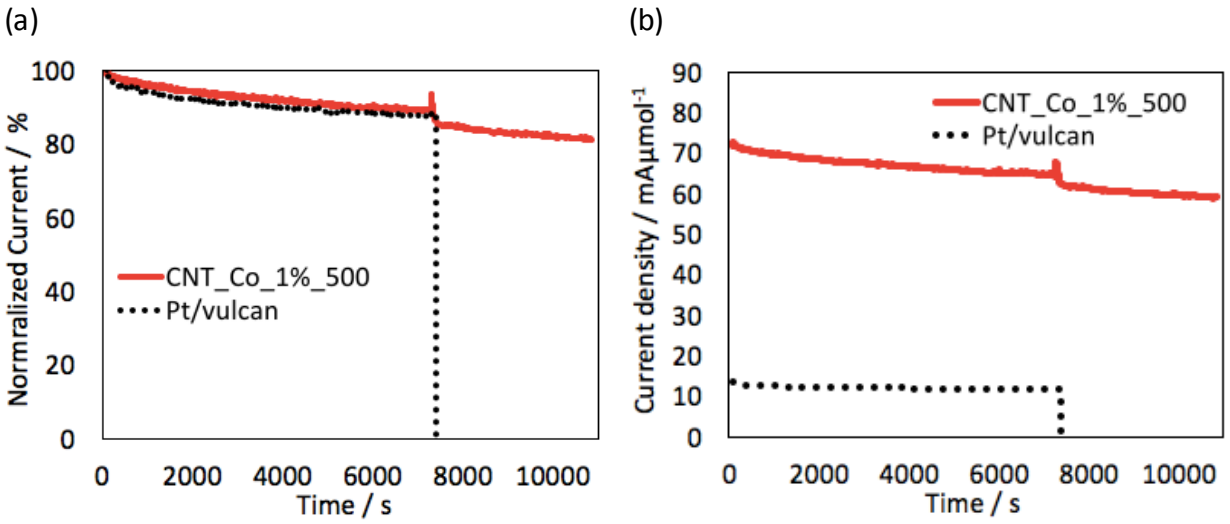

<InlineShape7>

Fig. 11. LSV curves for CNT_Co_1% and Pt/Vulcan before and after the cycling in O_2 - saturated 0.1M KOH solution at 1600rpm with a sweep rate of 5 mV s^{-1}. Catalyst loading is 400 μg/cm^2.

4. Conclusions

A facile method to synthesize Co NPs decorated CNTs catalysts which show efficient and stable activity for ORR was developed. Our catalyst containing 1 wt. % of Co NPs (average NPs: 8.9 nm) prepared with PVP as protecting agent and $NaBH_4$ has surprisingly high LC in alkaline solution which is similar to commercial Pt/Vulcan. The catalyst showed higher selectivity towards $4e^-$ electron pathway than CNT. Higher ORR activity is possible for smaller size of Co NPs catalysts due to the enlarged interfaces between Co species and CNTs. The addition of PVP and $NaBH_4$ during the preparation procedure is necessary for obtaining the highest activity since it

favors the formation of lower oxidation states for Co species and the formation of a N-doped carbon shell. The Co-containing catalysts with small particle sizes, low Co oxidation states and pyridinic N and quaternary N groups in the carbon framework seem to have the optimum combination to create the most active sites for this reaction. These results suggest that the synthesis of smaller particle sizes than those used in this study (below 8 nm) employing this preparation method can produce improved Co-based ORR catalysts and that this methodology could also be applied to other metal oxides to achieve improved ORR catalysts.

Acknowledgments

The authors would like to thank GV and FEDER (PROMETEOII/2014/010), projects CTQ2015-66080-R (MINECO / FEDER), MAT2016-76595-R (MINECO / FEDER), BES-2013-063678 and HEIWA NAKAJIMA FOUNDATION for the financial support.

Appendix A. Supplementary data

Supplementary data associated with this article can be found, in the online version at:

References

[1] C. Lamy, in:, E.F. François Béguin (Ed.), Carbons Electrochem. Energy Storage Convers. Syst., CRC Press, 2010, pp. 377–410.

[2] M. Winter, R.J. Brodd, Chem. Rev. 104 (2004) 4245–4270.

[3] F. Bidault, D.J.L. Brett, P.H. Middleton, N.P. Brandon, J. Power Sources 187 (2009) 39–48.

[4] N. Daems, X. Sheng, I.F.J. Vankelecom, P.P. Pescarmona, J. Mater. Chem. A 2 (2014) 4085–4110.

[5] Z. Yang, H. Nie, X. Chen, X. Chen, S. Huang, J. Power Sources 236 (2013) 238–249.

[6] K. Gong, F. Du, Z. Xia, M. Durstock, L. Dai, Science 323 (2009) 760–764.

[7] G. McLean, Int. J. Hydrogen Energy 27 (2002) 507–526.

[8] P. Trogadas, T.F. Fuller, P. Strasser, Carbon 75 (2014) 5–42.

[9] B. You, P. Yin, J. Zhang, D. He, G. Chen, F. Kang, H. Wang, Z. Deng, Y. Li, Sci. Rep. 5 (2015) 11739.

[10] G. Zhang, W. Lu, F. Cao, Z. Xiao, X. Zheng, J. Power Sources 302 (2016) 114–125.

[11] A. Pendashteh, J. Palma, M. Anderson, R. Marcilla, Appl. Catal. B Environ. 201 (2017) 241–252.

[12] T. Sun, L. Xu, S. Li, W. Chai, Y. Huang, Y. Yan, J. Chen, Appl. Catal. B Environ. 193 (2016) 1–8.

[13] P.W. Menezes, A. Indra, D. González-Flores, N.R. Sahraie, I. Zaharieva, M. Schwarze, P. Strasser, H. Dau, M. Driess, ACS Catal. 5 (2015) 2017–2027.

[14] Y. Liang, Y. Li, H. Wang, H. Dai, J. Am. Chem. Soc. 135 (2013) 2013–2036.

[15] C.H. Choi, M.W. Chung, H.C. Kwon, J.H. Chung, S.I. Woo, Appl. Catal. B Environ. 144 (2014) 760–766.

[16] S. Zhao, B. Rasimick, W. Mustain, H. Xu, Appl. Catal. B Environ. 203 (2017) 138–145.

[17] G. Wu, K.L. More, C.M. Johnston, P. Zelenay, Science 332 (2011) 443–447.

[18] M. Wang, J. Huang, M. Wang, D. Zhang, W. Zhang, W. Li, J. Chen, Electrochem. Commun. 34 (2013) 299–303.

[19] J. Xu, P. Gao, T.S. Zhao, Energy Environ. Sci. 5 (2012) 5333–5339.

[20] S.C. Hao, W.G. Uo, 29 (2013) 619–623.

[21] Y. Liang, Y. Li, H. Wang, J. Zhou, J. Wang, T. Regier, H. Dai, Nat. Mater. 10 (2011) 780–786.

[22] Q. He, Q. Li, S. Khene, X. Ren, F.E. López-Suárez, D. Lozano-Castelló, A. Bueno-López, G. Wu, J. Phys. Chem. C 117 (2013) 8697–8707.

[23] X. Yuan, L. Li, Z. Ma, X. Yu, X. Wen, Z.-F. Ma, L. Zhang, D.P. Wilkinson, J. Zhang, Sci. Rep. 6 (2016)

20005.

[24] J. Liu, L. Jiang, B. Zhang, J. Jin, D.S. Su, S. Wang, G. Sun, ACS Catal. 4 (2014) 2998–3001.

[25] Y. Liang, H. Wang, P. Diao, W. Chang, G. Hong, Y. Li, M. Gong, L. Xie, J. Zhou, J. Wang, T.Z. Regier, F. Wei, H. Dai, J. Am. Chem. Soc. 134 (2012) 15849–15857.

[26] L.M. Uhlig, G. Sievers, V. Brüser, A. Dyck, G. Wittstock, Sci. Bull. 61 (2016) 612–618.

[27] Y. Li, W. Zhou, H. Wang, L. Xie, Y. Liang, F. Wei, J.-C. Idrobo, S.J. Pennycook, H. Dai, Nat. Nanotechnol. 7 (2012) 394–400.

[28] C.W.B. Bezerra, L. Zhang, K. Lee, H. Liu, A.L.B. Marques, E.P. Marques, H. Wang, J. Zhang, Electrochim. Acta 53 (2008) 4937–4951.

[29] I. Miguel-García, Á. Berenguer-Murcia, T. García, D. Cazorla-Amorós, Catal. Today 187 (2012) 2–9.

[30] U.A. Paulus, T.J. Schmidt, H.A. Gasteiger, R.J. Behm, J. Electroanal. Chem. 495 (2001) 134–145.

[31] Y. Huang, M. Zhang, P. Liu, L. Wang, F. Cheng, Ionics 22 (2016) 1425–1432.

[32] D. Barreca, C. Massignan, S. Daolio, M. Fabrizio, C. Piccirillo, L. Armelao, E. Tondello, Chem. Mater. 13 (2001) 588–593.

[33] K. Niu, B. Yang, J. Cui, J. Jin, X. Fu, Q. Zhao, J. Zhang, J. Power Sources 243 (2013) 65–71.

[34] P. Bazylewski, D.W. Boukhvalov, A.I. Kukharenko, E.Z. Kurmaev, A. Hunt, A. Moewes, Y.H. Lee, S.O. Cholakh, G.S. Chang, RSC Adv. 5 (2015) 75600–75606.

[35] E. E. Raymundo-Pinero, D. Cazorla-Amoros, A. Linares-Solano, J. Find, U. Wild, R. Schlogl, Carbon 40 (2002) 597–608.

[36] E. Raymundo-Pinero, D. Cazorla-Amoros, A. Linares-Solano, Carbon 41 (2003) 1925–1932.

[37] I.G. Casella, M. Contursi, J. Solid State Electrochem. 16 (2012) 3739–3746.

[38] H.J. Pan, C.Y. Lin, U.S. Mohanty, J.H. Chou, Mater. Sci. Appl. 2 (2011) 1480–1484.

[39] J. Liu, L. Jiang, Q. Tang, B. Zhang, D.S. Su, S. Wang, G. Sun, ChemSusChem 5 (2012) 2315–2318.

[40] A. Bonakdarpour, M. Lefevre, R. Yang, F. Jaouen, T. Dahn, J.-P. Dodelet, J.R. Dahn, Electrochem.

Solid-State Lett. 11 (2008) B105–B108.

[41] Y. Dong, K. He, L. Yin, A. Zhang, Nanotechnology 18 (2007) 435602–435608.

[42] J. Xiao, Q. Kuang, S. Yang, F. Xiao, S. Wang, L. Guo, Sci. Rep. 3 (2013) 2300–2307.

[43] M. Wang, Y. Hou, R.C.T. Slade, J. Wang, D. Shi, D. Wexler, H. Liu, J. Chen, Front. Chem. 4 (2016) 1–10.

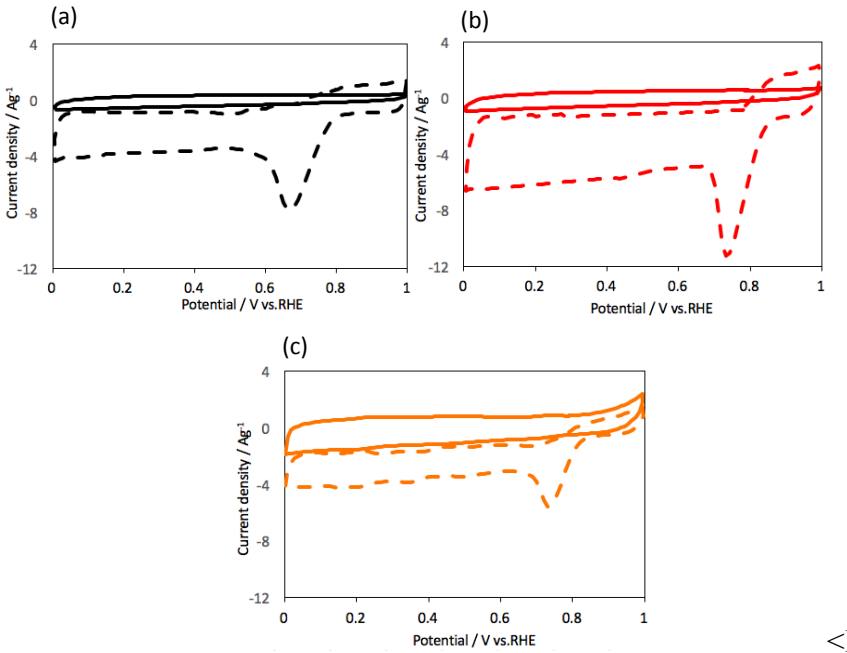

<InlineImage2>

Fig. 3. Steady state voltammograms for (a) CNT, (b) CNT_Co_1%_500 and (c) CNT_Co_17%_500 catalysts in N_2 (solid line) and O_2-saturated (dash line) 0.1M KOH solution at 50mVs^{-1} respectively. Catalyst loading is 400 µg/cm^2.

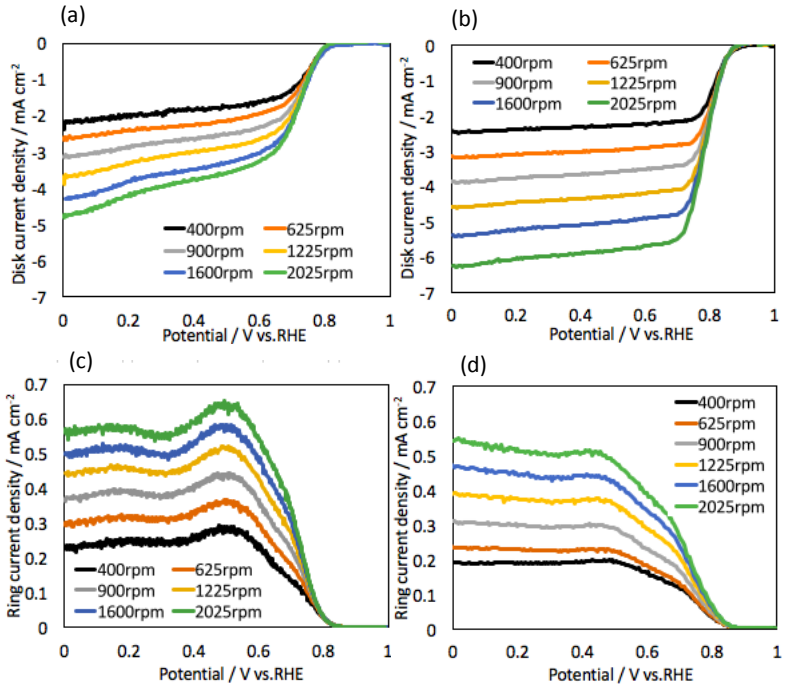

<InlineImage3>

Fig. 4. LSVs during ORR for (a) CNT and (b) CNT_Co_1%_500 and ring currents divided by collection efficiency for the (c) CNT and (d) CNT_Co_1%_500 in O_2 - saturated 0.1M KOH solution with a sweep rate of 5 mV/s respectively. Catalyst loading is 400 µg/cm^2.

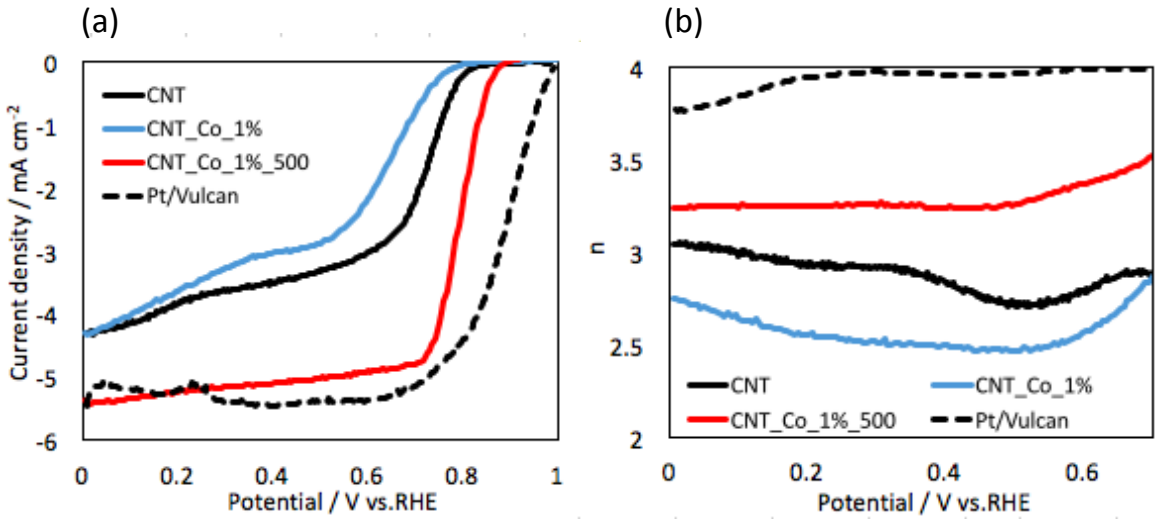

<InlineImage4>

Fig. 5. (a) LSVs during ORR on the disk electrode and (b) electron transfer number (n) of the CNT, CNT_Co_1%, CNT_Co_1%_500 and Pt/Vulcan in O_2 - saturated 0.1M KOH solution at 1600 rpm with a sweep rate of 5 mV/s respectively. Catalyst loading is 400 µg/cm^2.

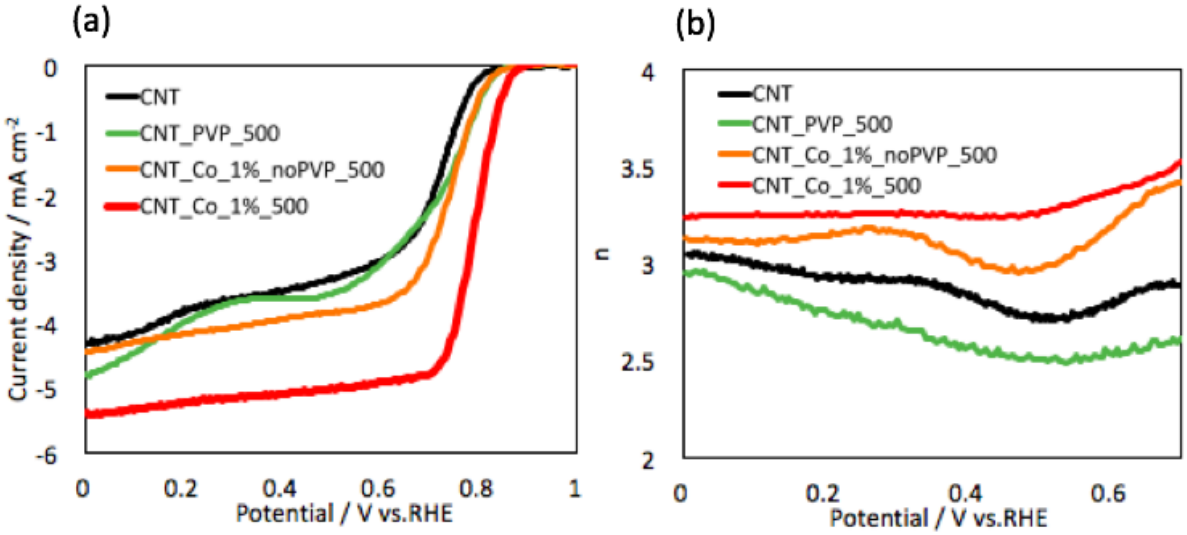

<InlineImage5>

Fig. 6. (a) LSVs during ORR on the disk electrode and (b) n of the CNT, CNT_PVP_500, CNT_Co_1%_noPVP_500 and CNT_Co_1%_500 in O_2 - saturated 0.1M KOH solution at 1600rpm with a sweep rate of 5 mV/s respectively. Catalyst loading is 400 µg/cm^2.

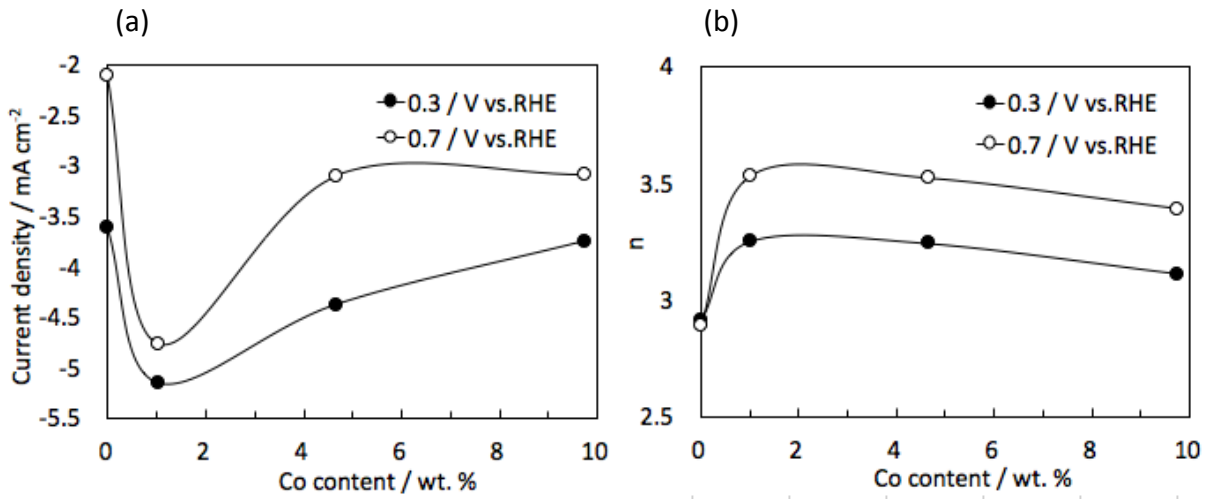

<InlineImage6>

Fig. 7. Relationship between Co content and (a) LC as well as (b) n measured at 0.3 V and 0.7 V vs.RHE in O_2 - saturated 0.1M KOH solution at 1600 rpm. Catalyst loading is 400 μg/cm^2. These catalysts were prepared with PVP and $NaBH_4$.

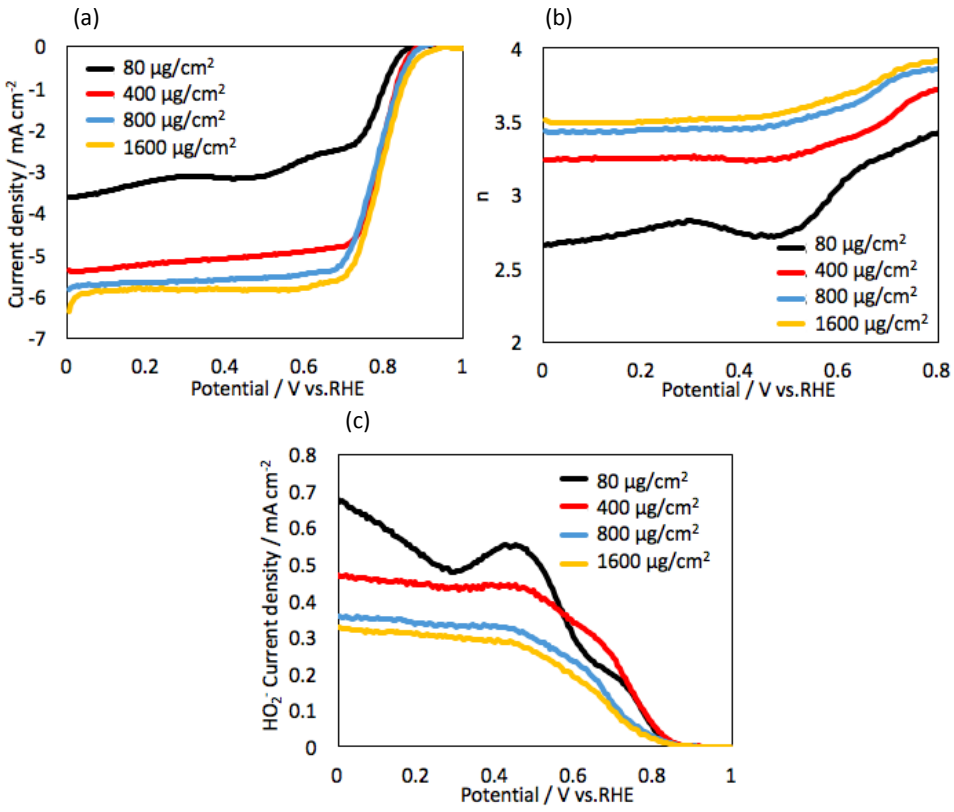

<InlineImage7>

Fig. 8. (a) LSVs for ORR on the disk electrode, (b) n and (c) ring current of CNT_Co_1%_500 with different loadings in O_2 - saturated 0.1M KOH solution at 1600 rpm with a sweep rate of 5 mV/s respectively.

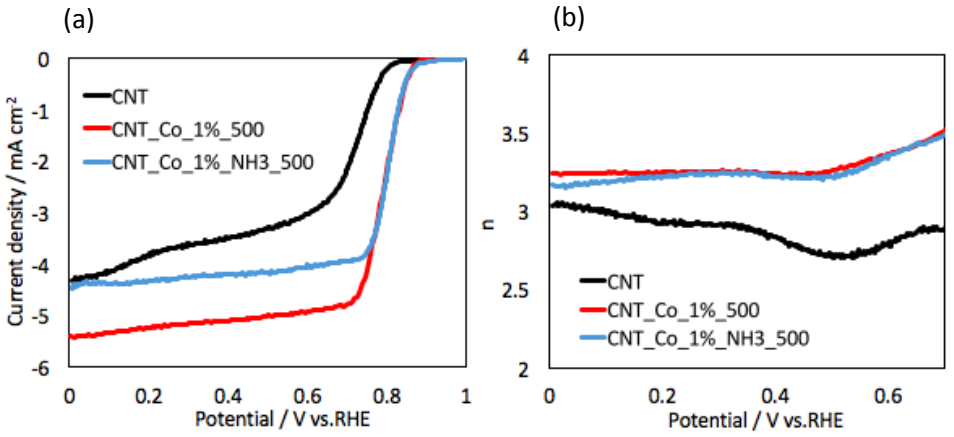

<InlineImage8>

Fig. 9. (a) LSVs during ORR on the disk electrode and (b) n of the CNT, CNT_Co_1% and CNT_Co_1%_NH_3_500 in O_2 - saturated 0.1M KOH solution at 1600rpm with a sweep rate of 5 mV/s respectively. Catalyst loading is 400 µg/cm^2.

<InlineShape6>

Fig. 10. Current versus time for CNT_Co_1% and Pt/Vulcan at 0.65V vs. RHE in O_2 - saturated 0.1M KC

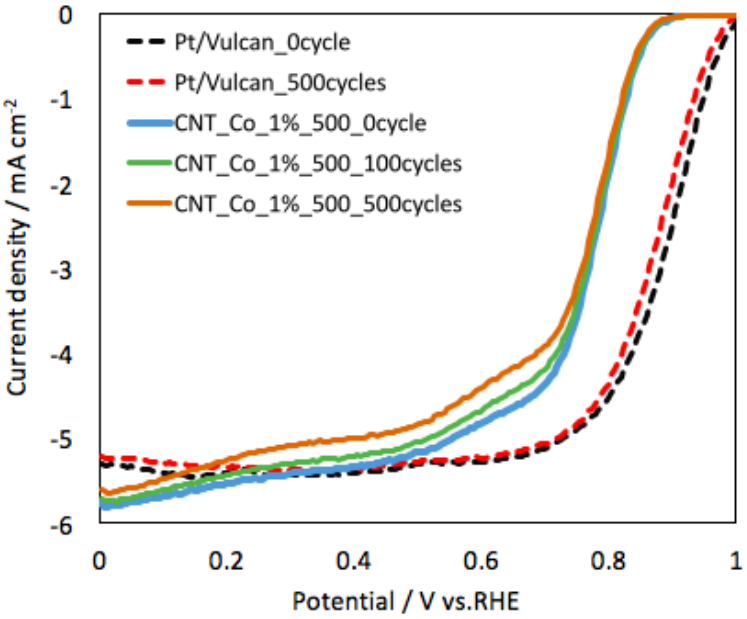

n normalized current base an 0 µg/cm^2.

Table 1

Composition of Co NT_Co_1%_500, CNT_Co_9%_500 an

Table 2

N atomic composition obtained from XPS and content of different N species for CNT, CNT_Co_1%_500, CNT_Co_9%_500, CNT_Co_17%_500, CNT_Co_1%_NH_3_500 and CNT_Co_1%_noPVP_500.

Sample	N / at. %	Quaternary N / %	Pyrrolic/pyridonic N / %	Pyridinic N / %
CNT	0	--	--	--
CNT_Co_1%_500	0.77	24.8	30.0	45.2
CNT_Co_9%_500	0.77	26.8	30.3	42.9
CNT_Co_9%_500	4.7			
CNT_Co_17%_500	8.2			

CNT_Co_17%_500	0.99	24.4	31.9	43.7
CNT_Co_1%_NH_3_500	0.28	17.1	53.5	29.4
CNT_Co_1%_noPVP_500	0	--	--	--

<InlineShape4>